Available online at www.sciencedirect.com
SCIENCE DIRECT®
Journal of Magnetic Resonance 159 (2002) 68–75
JMR Journal of Magnetic Resonance
www.academicpress.com

Gradient echo imaging of flowing hyperpolarized nuclei: theory and phantom studies on ^{129}Xe dissolved in ethanol

E. Johansson,[a,*] J. Svensson,[b] S. Månsson,[c] J.S. Petersson,[d] L.E. Olsson,[b] K. Golman,[d] and F. Ståhlberg[a,e]

[a] *Department of Radiation Physics, Lund University Hospital, Lund S-221 85, Sweden*
[b] *Department of Radiation Physics, Malmö University Hospital, Malmö, Sweden*
[c] *Department of Experimental Research, Malmö University Hospital, Malmö, Sweden*
[d] *Amersham Health R&D, Medeon, Malmö, Sweden*
[e] *Department of Diagnostic Radiology, Lund University Hospital, Lund S-221 85, Sweden*

Abstract

The influence of flip angle and flow velocity on the signal intensity achieved when imaging a hyperpolarized substance with a spoiled gradient echo sequence was investigated. The study was performed both theoretically and experimentally using hyperpolarized xenon dissolved in ethanol. Analytical expressions regarding the optimal flip angle with respect to signal and the corresponding signal level are presented and comparisons with thermally polarized substances are made. Both experimentally and theoretically, the optimal flip angle was found to increase with increasing flow velocity. Numerical calculations showed that the velocity dependence of the signal differs between the cases of hyperpolarized and thermally polarized substances.

Keywords: MRI; Hyperpolarization; Xenon; Flow; Gradient echo

1. Introduction

The polarization levels of ^{3}He and ^{129}Xe can be raised with optical pumping techniques by a factor of $\sim 10^5$ relative to that of thermal equilibrium at typical field strengths of clinical MRI scanners [1–3]. With the corresponding rise in signal, lung imaging has been investigated using ^{3}He [4,5] as well as ^{129}Xe [6,7], and the clinical potential of ^{3}He in particular has been demonstrated [8–10]. For study of the vascular system, hyperpolarized contrast agent techniques may form interesting alternatives to those used in conventional ^{1}H MRI. Helium has a low solubility in blood, but has been proposed for vascular studies using encapsulation techniques [11–14]. Xenon, on the other hand, is directly soluble in blood, and inhalation [7,15,16] of the gas is one way of administering hyperpolarized xenon to the human vascular system. Regrettably, ^{129}Xe has a relatively short longitudinal relaxation time (5–10 s) in blood [17]. It has been proposed that xenon should be dissolved prior to injection in a biocompatible carrier in which the relaxation time is longer and the solubility even higher than in blood [18]. Examples of such carriers are lipid emulsions [19,20] and perfluorocarbon emulsions [21]. Recently, other nuclei suitable for hyperpolarization have also been proposed for vascular studies. For example, the potential of hyperpolarized ^{13}C for angiography has been investigated [22].

MRI using hyperpolarized substances differs in many respects from imaging with common thermally polarized substances. For instance, when employing a spoiled gradient echo sequence on a static sample, the longitudinal magnetization does not reach a steady-state level after a few RF excitations [23], as is the case for a thermally polarized substance where T1 relaxation causes a regrowth of magnetization. Instead, the longitudinal magnetization is constantly decreased with every RF pulse it experiences. However, if flowing nuclei are considered, the decrease in magnetization in the imaging slice will be counterbalanced by fresh magnetization. The resulting signal will depend on flip angle and flow

* Corresponding author. Fax: +46-46-127249.
E-mail address: edvin.johansson@radfys.lu.se (E. Johansson).

1090-7807/02/$ - see front matter © 2002 Elsevier Science (USA). All rights reserved.
PII: S1090-7807(02)00117-9

velocity, as in imaging of thermally polarized substances [24,25], but the signal levels will differ due to the different influence of longitudinal relaxation.

There have been few investigations of flow dependence of the signal from hyperpolarized nuclei imaged with a spoiled gradient echo sequence [19,26]. Gao et al. [26] have derived theoretical signal expressions for the plug flow case and Möller et al. [19] used a plug flow model for experimental determination of flow values in a rat model. To our knowledge, experimental verification and evaluation of signal expressions for the laminar flow case have not been presented before. The aim of this study was therefore to investigate the influence of flip angle and flow velocity on the signal when imaging a hyperpolarized substance dissolved in flowing liquid with a spoiled gradient echo sequence. The problem was treated theoretically as well as experimentally in a phantom model using hyperpolarized xenon dissolved in ethanol. Signal equations and expressions for the highest achievable signal in cases of plug flow and laminar flow are presented, together with expressions for the corresponding optimal flip angle. Comparisons with the case of thermal polarization are made through numerical calculation.

2. Theory

Signal expressions and expressions for the optimal flip angle and the corresponding signal are derived for the cases of plug flow and laminar flow. Relaxation is included in a different way in the signal expressions, compared with what was presented previously by Gao et al. [26].

A gradient echo sequence with repetition time TR, complete spoiling of transverse magnetization between repetition intervals, flip angle α, and slice thickness Δx is assumed. For plug flow of a hyperpolarized substance with the velocity v perpendicular to the imaging slice, the amount of signal, S_p, acquired after each RF excitation following a number of RF pulses larger than $n = \Delta x/vTR$ can be expressed as follows:

$$S_p(\alpha) = S_0 \sin\alpha \left[\frac{1}{n} \sum_{i=0}^{N-1} \cos^i \alpha + \left(1 - \frac{N}{n}\right) \cos^N \alpha \right] = S_0 \sin\alpha \left[\frac{1}{n} \frac{1-\cos^N \alpha}{1-\cos\alpha} + \left(1 - \frac{N}{n}\right) \cos^N \alpha \right]. \quad (1)$$

Longitudinal relaxation regrowth of the flipped magnetization is disregarded, since the polarization level is assumed to be many orders of magnitude greater than that at thermal equilibrium. During flow, the spins in the slice have experienced various numbers of RF excitation pulses and the expression is simply a summation of their contributions, as illustrated in Fig. 1. N is the truncated value of n and S_0 is the signal achieved from a hypothetical single 90° RF excitation pulse. S_0 is time dependent in a hyperpolarized substance with longitudinal relaxation time T1, i.e., $S_0 \propto e^{-t/T1}$. Gradient echo image acquisition times are in general short compared with the longitudinal relaxation time of hyperpolarized substances, making Eq. (1) also interpretable as the expected signal level in an acquired image. The signal expression can be approximated by substituting N with n, resulting in following equation

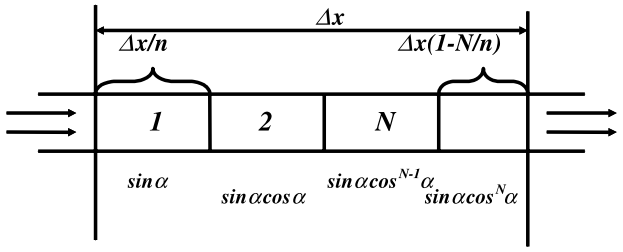

Fig. 1. Illustration of plug flow perpendicular to the imaging slice, used as motivation for Eq. (1), the signal expression. A hyperpolarized substance enters the slice from the left and as it experiences an increasing number of RF pulses (flip angle α) as it passes through the slice, its contribution to the total signal is decreased. n is defined as $\Delta x/vTR$, where Δx is the slice thickness, v the flow velocity, TR the repetition time, and N is the truncated value of n.

$$S_p(\alpha) = S_0 \frac{\sin\alpha}{n} \frac{1-\cos^n \alpha}{1-\cos\alpha}. \quad (2)$$

To find the optimal flip angle (the flip angle giving the highest value of the signal), Eq. (2) is differentiated with respect to α and set to equal zero

$$\cos^{n-1}\alpha\left(n\sin^2\alpha + \cos\alpha\right) - 1 = 0. \quad (3)$$

The solution to Eq. (3) converges towards the expression given in Eq. (4) as α decreases; k_p is a dimensionless constant, and α is expressed in radians

$$\alpha = k_p \sqrt{\frac{1}{n}} = k_p \sqrt{\frac{vTR}{\Delta x}}. \quad (4)$$

It can be shown that k_p must be the solution to Eq. (5). Solved numerically, this gives $k_p = 1.585\ldots$

$$e^{k_p^2/2} - k_p^2 - 1 = 0. \quad (5)$$

For a more detailed analysis of the steps leading to Eqs. (4) and (5), the reader is referred to Appendix A. With the substitution of α in Eq. (2) with Eq. (4), the expression for the highest achievable amount of signal, the following equation is reached

$$S_p = S_0 \left(\frac{2k_p^2}{1+k_p^2} \right) \sqrt{\frac{vTR}{\Delta x}}. \quad (6)$$

In Eq. (6), two approximations have been made. Firstly, N is assumed to equal n and secondly, the solution of Eq. (3) is approximated by the flip angle value in Eq. (4), which is the result of a low angle approximation.

In the case of fully developed laminar flow of a hyperpolarized substance in the through-plane direction in a vessel with circular cross-section, the signal expression can be formulated as in Eq. (7), where $f(v)$ is the velocity distribution function in a cross-section of the vessel. In contrast to the plug flow case, the signal may only reach this level asymptotically, since spins having practically zero velocity might be included

$$S_{\mathrm{l}}(\alpha) = \int f(v) S_{\mathrm{p}}(v,\alpha)\,\mathrm{d}v. \tag{7}$$

The velocity distribution function (the function describing the density of spins with a certain velocity in the slice), $f(v)$, of laminar flow in a tube with circular cross-section can be expressed as Eq. (8), where v_0 is the mean flow velocity of the fluid [27]

$$f(v) = \frac{1}{2v_0} \quad (0 \leqslant v \leqslant 2v_0). \tag{8}$$

A complicating factor emerges when a fluid is injected into a flowing medium having a laminar flow profile. In this case, the velocity distribution function of the injected substance in the imaging slice will generally not be identical to the velocity distribution function of *all* fluid in the slice. The velocity distribution function of the injected substance in the slice will vary with time as the injected fluid passes by. Given that the slice thickness is small compared with l, the distance between the point of injection and the imaging slice, and assuming an instantaneous injection at the time $t = 0$ the velocity distribution function can be expressed as Eq. (9). V is the injected volume and r_0 the vessel radius

$$f(v,t) = \begin{cases} \frac{1}{2v_0} & \text{if } \frac{l}{v} < t < \frac{l}{v} + \frac{V}{\pi r_0^2 v}, \\ 0 & \text{otherwise.} \end{cases} \quad (0 \leqslant v \leqslant 2v_0) \tag{9}$$

By integrating $f(v,t)$ over all velocities and differentiating with respect to t, it can be demonstrated that the highest amount of injected fluid in the slice is expected just as the last spins with the highest velocity are leaving the slice. The velocity distribution function at this particular moment is given by

$$f(v) = \begin{cases} \frac{1}{2v_0} & \text{if } \frac{2v_0}{1+(V/l\pi r_0^2)} < v < 2v_0, \\ 0 & \text{otherwise.} \end{cases} \tag{10}$$

Eq. (10) will be used later when comparisons with experimental results are made, but when deriving analytical expressions similar to Eqs. (4) and (6) for the laminar case, Eq. (8) was used for the sake of generality. Hence, the assumption was made that the whole vessel consisted of the injected substance. In order to obtain the optimal flip angle, Eq. (7) was differentiated with respect to α and solved for zero as in the plug flow case, leading to the following equation:

$$\int_0^{2v_0} \left[\cos^{n-1}\alpha \left(\sin^2\alpha + \frac{\cos\alpha}{n} \right) - \frac{1}{n} \right] \mathrm{d}v = 0. \tag{11}$$

With the same approximations as in the plug flow case, Eq. (11) can be solved for the optimal flip angle: Eq. (12). For further details, see Appendix A

$$\alpha = k_{\mathrm{l}} \sqrt{\frac{v_0 TR}{\Delta x}}. \tag{12}$$

The dimensionless constant k_{l} is the solution to Eq. (13) and can be determined numerically to $k_{\mathrm{l}} = 1.652\ldots$

$$\int_0^1 \left[\mathrm{e}^{-k_{\mathrm{l}}^2/4z} \left(\frac{k_{\mathrm{l}}^2}{2} + z \right) - z \right] \mathrm{d}z = 0. \tag{13}$$

Under the assumptions stated above, the signal achieved when employing the optimal flip angle in the laminar case is given by Eq. (14)

$$S_{\mathrm{l}} = S_0 \frac{8}{3} \frac{1 - \mathrm{e}^{-k_{\mathrm{l}}^2/4}}{k_{\mathrm{l}}} \sqrt{\frac{v_0 TR}{\Delta x}}. \tag{14}$$

So far, relations for achieving the highest amount of signal have been derived for the through-plane situation. If the vessel is oriented within the slice, the formalism can still be applied with Δx taken as the vessel path length in the imaging plane. Note that the path does not have to run straight through the slice. In-plane images will have a noticeable signal gradient in the direction of the flow, since spins in the outflow part of the slice have experienced more RF pulses. This signal loss will be independent of other imaging parameters when the flip angles derived earlier, Eqs. (4) and (12), are used. The drops in signal are calculated for plug flow (κ_{p}) and laminar flow (κ_{l}) in Eqs. (15) and (16). These are defined as the ratio between the signal from the hyperpolarized substance having just entered the slice and of that just about to leave it. In the derivation, Eq. (3) is used in the plug flow case, and Eq. (11) in the laminar case

$$\kappa_{\mathrm{p}} = \cos^{n-1}\alpha \approx \frac{1}{1 + k_{\mathrm{p}}^2} = 0.285\ldots, \tag{15}$$

$$\kappa_{\mathrm{l}} = \frac{1}{2v_0} \int_0^{2v_0} \cos^{n-1}\alpha\,\mathrm{d}v \approx \frac{4}{3} \frac{1 - \mathrm{e}^{-k_{\mathrm{l}}^2/4}}{k_{\mathrm{l}}^2} = 0.242\ldots \tag{16}$$

3. Materials and methods

Xenon of natural abundance was polarized using a commercial polarizer (IGI. 9600 Xe, Amersham Health, Durham, NC). The polarized gas was stored in a 200 ml glass cell at a pressure of about 3 atm. The polarized xenon was dissolved in ethanol (95%), which has high solubility of xenon (Ostwald coefficient 2.5 at 20 °C [28]), low viscosity (1.2 m Pa s) and in which xenon has

long T1 relaxation time (estimated to 50 s at 2.4 T in a non-deoxygenized solution). By vigorous shaking, 30 ml of the high-pressure gas was mixed with 30 ml of ethanol in a syringe.

In the experiments, a flow of ethanol was established through the magnet (2.4 T, Bruker Biospec 24/30; Bruker Medical GmbH, Ettlingen, Germany) using gravity fall from a reservoir and a soft PVC tube with an inner diameter of 4 mm. During each experiment, 25 ml of the xenon solution was injected 65 cm upstream of the magnet isocenter. Through-plane images were acquired with three different mean flow velocities: 14, 21, and 36 cm/s. The velocities were estimated with a stop clock and measuring glass. A gradient echo sequence, $TR/TE = 12/6$ ms, with gradient spoiling was used to acquire axial slices with a slice thickness of 10 mm. The FOV was 6×4.5 cm and the matrix 64×32, resulting in a voxel size of $0.9 \times 1.4 \times 10\,\text{mm}^3$. The total acquisition time was 384 ms.

The flip angle dependency was investigated by acquiring consecutive images with different flip angles on the same injection. Since the amount of xenon present in the imaging slice varies with time if laminar flow is assumed, it was of importance that the separation in time of images acquired with different flip angles was limited. As a consequence, only three different flip angles were acquired from each injection in two repeated flip angle sets, 10°–30°–50° and 50°–70°–90°. Imaging was performed continuously as the injected fluid passed through the magnet and three adjacent images at the maximum signal-to-noise-ratio (SNR) were selected retrospectively. Ideally, at the time-point when these images are acquired, the velocity distribution function of the hyperpolarized xenon in the slice is described by Eq. (10). In each image, the mean intensity of the pixels in the tube and the mean intensity of the pixels in a large area outside of the tube were calculated. The SNR in the tube was calculated using the formalism for low SNR values [29]. The SNRs of the selected images were normalized to the image in each of the two series acquired with the flip angle 50°. The results of the experimental measurements were also compared with theoretical signal expressions for the laminar flow case. The flip angle dependency of the signal relative to S_0 for the three mean flow velocities was calculated using Eq. (7) together with the laminar velocity distribution function of the injected hyperpolarized substance from Eq. (10).

A series of in-plane images was also acquired. In this case, isotopically enriched xenon (75% ^{129}Xe) was used. The FOV was 6×6 cm, 64×32 matrix, flow velocity 18 cm/s, TR/TE 10/6 ms, flip angle 25°, and the vessel radius was 3 mm.

The velocity dependences of the signal from a hyperpolarized substance with long T1 and a thermally polarized substance with short T1 were compared by numerical computation. T1 was set to 50 ms in the thermal case, corresponding to that of blood when using a typical contrast agent in standard ^{1}H CE-MRA, whereas the only assumption regarding the hyperpolarized case was that T1 was long compared with the image acquisition time. The exact value of T1 is not of importance since with this assumption, the signal relative to S_0 does not depend on T1. The signal was calculated using Eq. (7) for the hyperpolarized substance and the signal equations described in [24] for the thermally polarized substance. The comparisons were performed assuming a tube with full laminar flow (Eq. (8)), $\Delta x = 10$ mm, $TR = 12$ ms, and flip angle 30°, corresponding to a through-plane imaging situation. The signal relative to S_0 was calculated in a mean flow velocity interval of 0–50 cm/s, where again S_0 is defined as the signal achieved from a hypothetical single 90° RF excitation. The optimal flip angle in the same velocity interval was also calculated using Eq. (12) in the hyperpolarized case, and by stepping the flip angle in small increments for a given mean flow velocity and evaluating the signal in the thermal case.

4. Results

The correspondence between measured and theoretical signal values as a function of flip angle for the three different mean velocities is shown in Fig. 2, and the optimal flip angle is increasing experimentally as well as theoretically for increasing flow velocity.

For the in-plane case, the expected signal drop in the direction of the flow is visible in Fig. 3. The image is the

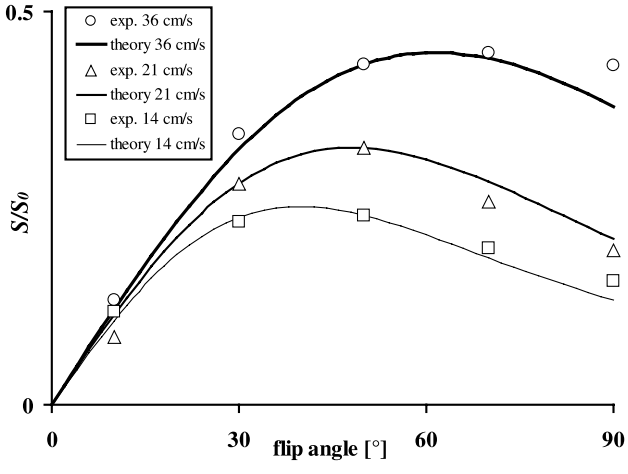

Fig. 2. The experimentally and theoretically determined signal relative to S_0 dependency on flip angle at 14, 21, and 36 cm/s, when imaging hyperpolarized xenon dissolved in ethanol with a spoiled gradient echo sequence. The experimental results are scaled to the corresponding theoretically acquired result at flip angle 50°. The slice thickness was 10 mm and the repetition time 12 ms. Eq. (7) and the laminar velocity distribution function described by Eq. (10) were used to calculate the theoretical dependence.

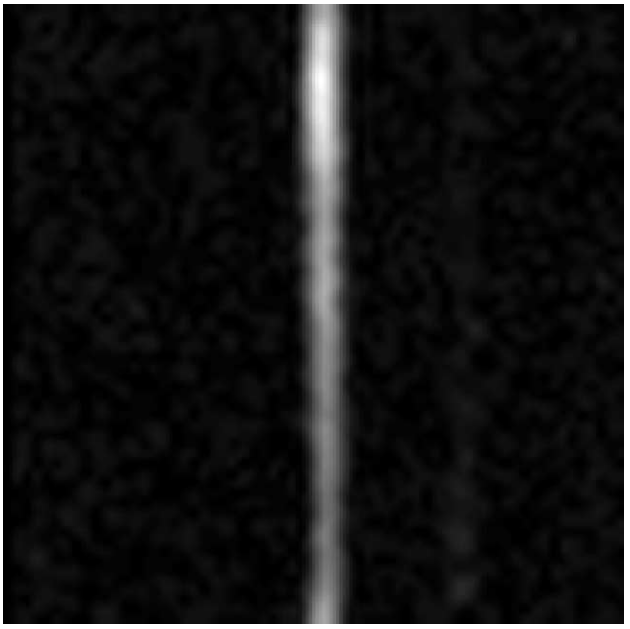

Fig. 3. In-plane image of flowing (18 cm/s) hyperpolarized dissolved xenon. The image was obtained by averaging 21 consecutive gradient echo images with TR 10 ms and flip angle 25°. The direction of flow is from top to bottom.

result of raw-data averaging of 21 consecutively acquired coronal images.

The velocity dependence of the signal relative to S_0 in a typical through-plane situation with laminar flow is more pronounced in the case of the hyperpolarized substance (Fig. 4) than in the case of a thermally polarized substance. At low velocities, the signal from the hyperpolarized substance increases rapidly when the velocity is increased. The optimal flip angle for the hyperpolarized fluid is found to be lower than that of a thermally polarized fluid, but the difference decreases when the mean flow velocity is increased; see Fig. 5.

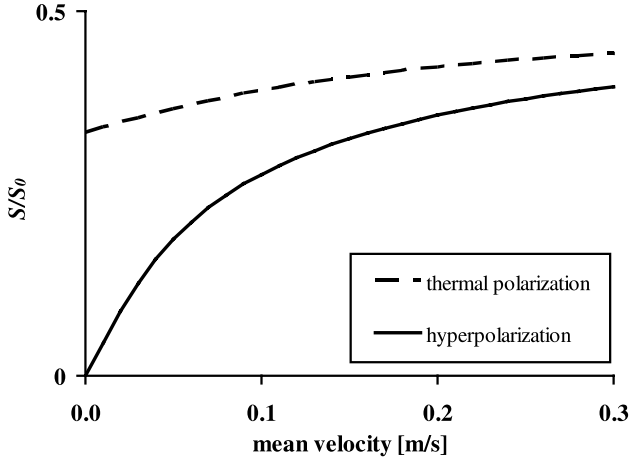

Fig. 4. The calculated velocity dependence of the signal for a thermally polarized substance (T1 50 ms) and a hyperpolarized substance (long T1). The signals relative to S_0 (defined as the signal achieved from a hypothetical single 90° RF excitation) are plotted against the mean flow velocity assuming laminar flow. The assumed slice thickness was 10 mm, the repetition time 12 ms, and the flip angle 30°.

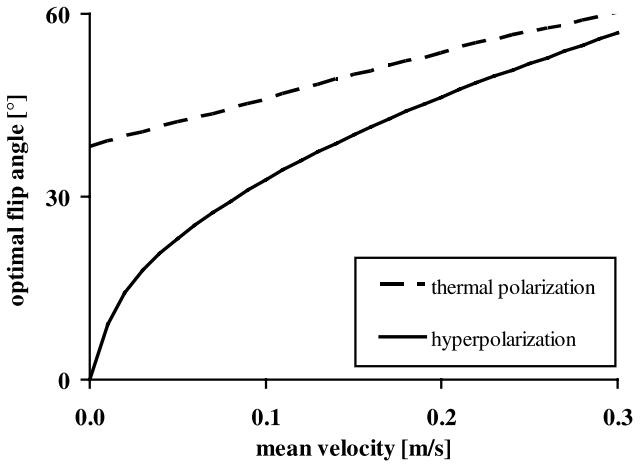

Fig. 5. The calculated optimal flip angle as a function of mean flow velocity assuming laminar flow, slice thickness 10 mm, and a repetition time of 12 ms for a thermally polarized substance (T1 50 ms) and a hyperpolarized substance (long T1).

The expressions derived for optimal flip angle and signal for plug flow (Eqs. (4) and (6)) and laminar flow (Eqs. (12) and (14)) differ by a constant factor. In general, a slightly higher flip angle (4%) is required to image laminar flow optimally and the resulting signal strength is slightly lower (12%) compared with imaging of plug flow with the same mean flow velocity. In both cases, the signal depends on the square root of the flow velocity and the repetition time. For through-plane flow, S_0 itself is linearly dependent on the slice thickness, and if this is taken into account, the signal also depends linearly on the square root of the slice thickness.

5. Discussion

Imaging with hyperpolarized substances in the vascular system is attractive for a number of reasons, mainly due to the high contrast expected between vascular structures and background tissue. Implementation of the hyperpolarization technique may lead to fundamentally new methods for performing MR angiography [12,22], quantitative flow measurements [19] and perfusion measurements [14,20,30]. The success of the techniques will depend largely on the achieved level of polarization of the nuclei and, when carriers are needed, their properties [18]. However, the search for suitable imaging sequences and their basic flow properties are certainly also important.

In this study, we have investigated the signal acquired with a spoiled gradient echo sequence when imaging a flowing hyperpolarized substance. Experimental work has been performed on xenon dissolved in ethanol, but the results of this study apply to all hyperpolarized

substances whose movements can be characterized as either plug or laminar flow. The key assumption in the derivation of the relations is that the polarization level is several orders of magnitude greater than that of thermal equilibrium. When this requirement is fulfilled, regrowth of spoiled magnetization can be ignored, making Eq. (1) valid. Note that for a thermally polarized substance with a long T1, the same argument can be claimed, making the results of the derivations valid also in this case.

For through-plane flow, by making multiple measurements on the same injected hyperpolarized liquid within a short period of time, it was possible to compare the signal in consecutively acquired images with theoretical values of the optimal flip angle. Except for the time separation between measurements, additional possible error sources in the measurement procedure are imperfect spoiling of transversal magnetization between excitations, imperfect slice selection, and the influence of noise. The experimental results agree with those expected according to theory, indicating rather high optimal flip angles even at moderate flow velocities, as have been reported earlier for the plug flow case [26]. For in-plane flow, the signal drop in the flow direction of an in-plane image is unavoidable when a constant flip angle approach is used. With the flip angle yielding the highest possible total signal in the image, the signal drop is substantial. By decreasing the flip angle, this effect can be mediated at the cost of a lower total amount of signal in the image.

From Figs. 4 and 5 it can be seen that the relative signal at a fixed flip angle, as well as at the optimal flip angle as a function of flow velocity, in the hyperpolarized and the thermal cases, resemble each other at higher flow velocities. The signal in the hyperpolarized case drops to zero when the flow velocity is decreased, whereas for $v = 0$ in the thermal case, the signal is governed by the signal equation for stationary matter with the assumed relaxation and imaging parameters. This may seem erroneous, since imaging of a non-flowing hyperpolarized substance is by no means impossible. However, it should be pointed out that Fig. 4 illustrates the signal acquired after $n\ (= \Delta x/vTR)$ RF pulses emitted and the theory given above is not applicable in the case when the velocity approaches zero.

An additional observation can be made from the derived signal expressions for hyperpolarized nuclei. Consider the situation where it is of interest to achieve the highest SNR in a specified amount time. The SNR is proportional to the square root of the number of times a measurement is repeated, which is proportional to TR^{-1}. Consequently, for a fixed readout time, according to the derived signal expressions the maximal signal level will be independent of TR as long as the optimal flip angle is employed. Since a long TR allows a longer readout time and thus a lower bandwidth, a long TR might be advantageous as long as $T2^*$ relaxation is not too severe.

6. Conclusion

This study discusses one of the most basic MR imaging sequences, the gradient echo, for which basic flow dependence was investigated theoretically and experimentally in a simple phantom model, using hyperpolarized ^{129}Xe dissolved in ethanol. For the cases of plug and laminar flow, basic equations were used to derive analytical expressions for optimal flip angle and signal. Although the experimental part of this study was performed with ^{129}Xe, the conclusions are applicable to the general case of flow of hyperpolarized nuclei such as ^{3}He and ^{13}C.

Acknowledgments

This study was supported in part by the Swedish Cancer Foundation, Grant No. 3806-B0005XAA.

Appendix A

In the plug flow case, we seek the solution to $\cos^{n-1}\alpha(n\sin^2\alpha + \cos\alpha) = 1$, which can be rewritten as

$$e^{-n\ln\cos\alpha} - 1 - n\frac{\sin^2\alpha}{\cos\alpha} = 0.$$

By setting $\lambda = -n\ln\cos\alpha$, and dividing by λ

$$\frac{e^{\lambda} - 1}{\lambda} + \frac{\sin^2\alpha}{\cos\alpha\ln\cos\alpha} = 0$$

is reached. The trigonometric term can be Taylor expanded as

$$\frac{\sin^2\alpha}{\cos\alpha\ln\cos\alpha} = -2 - \frac{\alpha^4}{12} + O(\alpha^6),$$

where α is expressed in radians. We have thus shown that when α is small, the solution sought is given by $\lambda = -n\ln\cos\alpha$, where λ is defined by $((e^{\lambda} - 1)/\lambda) - 2 = 0$. This can be determined numerically to $1.256\ldots$

We introduce the relation $k_p = \sqrt{2\lambda} = 1.585\ldots$, and $\lambda = -n\ln\cos\alpha$ can be approximated further using $\ln\cos\alpha \approx -\alpha^2/2$, into the simplified expression $\alpha = k_p\sqrt{1/n}$.

Regarding laminar flow, we begin with the relation

$$\int_0^{2v_0}\left[\cos^{n-1}\alpha\left(\sin^2\alpha + \frac{\cos\alpha}{n}\right) - \frac{1}{n}\right]dv = 0,$$

where n is velocity dependent as it is defined by $n = \Delta x/vTR$. By assuming

$$\lambda = -\frac{\Delta x}{v_0 TR}\ln\cos\alpha$$

and with the substitution $z = v/2v_0$, the expression

$$\int_0^1\left[e^{-\lambda/2z}\left(\frac{\sin^2\alpha}{\cos\alpha\ln\cos\alpha}\lambda - 2z\right) + 2z\right]dz = 0$$

is reached. Again, we use the same Taylor expansion and conclude that when α is small,

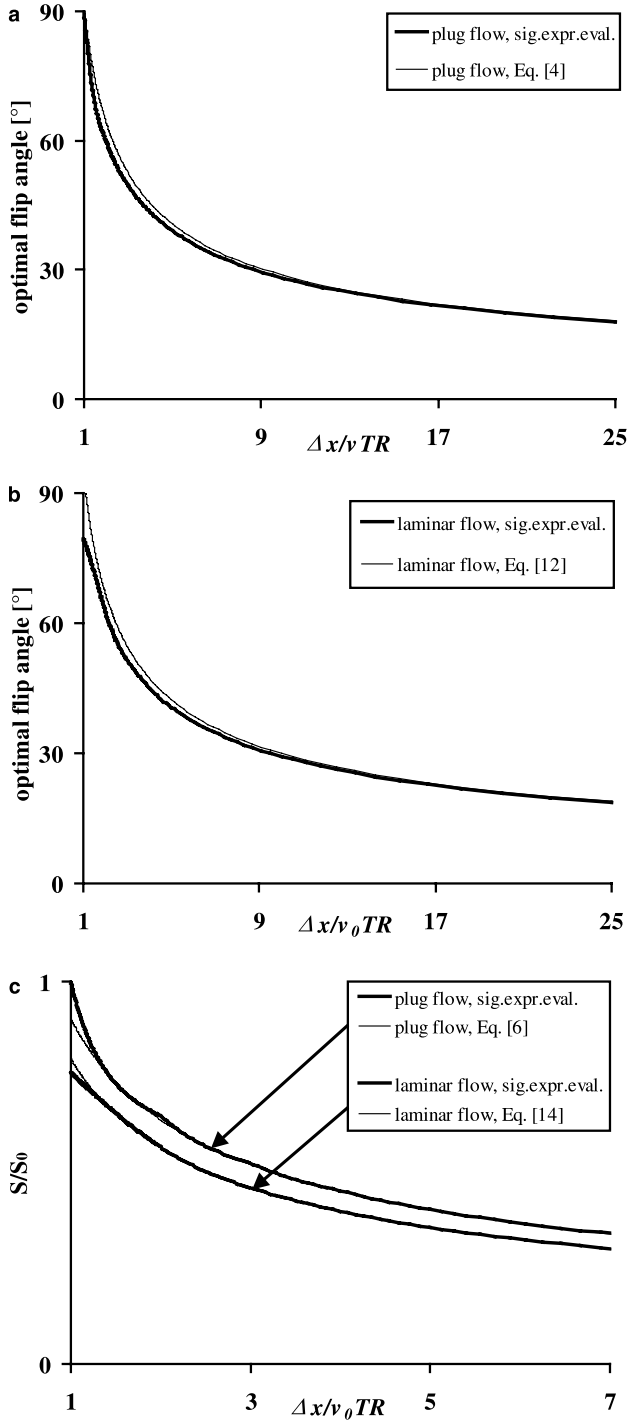

Fig. 6. Validation of the derived approximate expressions for optimal flip angle (a,b) and highest achievable signal (c) for plug and laminar flow as a function of the average number of RF pulses experienced when passing through the imaging slice. The derived expressions, Eqs. (4), (6), (12), and (14), are compared with the corresponding values found by evaluating the signal expressions (Eqs. (1) and (7)) for varying mean flow velocity and flip angle.

$$\lambda = -\frac{\Delta x}{v_0 TR}\ln\cos\alpha$$

is the solution sought, where λ is a constant found by solving

$$\int_0^1 [e^{-\lambda/2z}(\lambda + z) - z]\,dz = 0.$$

The rest of the derivation is identical to that of the plug flow case.

The validity of the derived expressions for the optimal flip angle and signal in the cases of plug and laminar flow was also investigated, since approximations were performed to obtain these expressions. This was done by comparing the derived expressions for optimal flip angle and signal with values found by evaluating the signal expressions, Eqs. (1) and (7), for varying mean flow velocity and flip angle. The derived expressions and those obtained by evaluating the signal expressions only differ at high velocities (Fig. 6). When more relevant parameter settings are considered, i.e., conditions in which a flowing nucleus experiences multiple RF excitations, the difference is decreased.

References

[1] W. Happer, E. Miron, S. Shaefer, D. Schreiber, W. Wijngaarden, X. Zeng, Polarization of the nuclear spins of noble-gas atoms by spin exchange with optically pumped alkali-metal atoms, Phys. Rev. A Gen. Phys. 29 (1984) 3092–3110.

[2] T. Chupp, M. Wagshul, K. Coulter, A. McDonald, W. Happer, Polarized high-density gaseous ^{3}He targets, Phys. Rev. C Nucl. Phys. 36 (1987) 2244–2251.

[3] B. Driehuys, G.D. Cates, E. Miron, K. Sauer, D.K. Walter, W. Happer, High-volume production of laser-polarized ^{129}Xe, Appl. Phys. Lett. 69 (1996) 1668–1670.

[4] H.-U. Kauczor, D. Hofmann, K.-F. Kreitner, H. Nilgens, R. Surkau, W. Heil, A. Potthast, M.W. Knopp, E.W. Otten, M. Thelen, Normal and abnormal pulmonary ventilation: visualization at hyperpolarized He-3 MR imaging, Radiology 201 (1996) 564–568.

[5] H.-U. Kauczor, M. Ebert, K.-F. Kreitner, H. Nilgens, R. Surkau, W. Heil, D. Hofmann, E.W. Otten, M. Thelen, Imaging of the lungs using ^{3}He MRI: preliminary clinical experience in 18 patients with and without lung disease, J. Magn. Reson. Imaging 7 (1997) 538–543.

[6] M.S. Albert, G.D. Cates, B. Driehuys, W. Happer, B. Saam, C.S. Springer Jr., A. Wishner, Biological magnetic resonance imaging using laser-polarized ^{129}Xe, Nature 370 (1994) 199–201.

[7] J.P. Mugler III, B. Driehuys, J.R. Brookeman, G.D. Cates, S.S. Berr, R.G. Bryant, T.M. Daniel, E.E. De Lange, J.H. Downs III, C.J. Erickson, W. Happer, D.P. Hinton, N.F. Kassel, T. Maier, C.D. Philips, B.T. Saam, K.L. Sauer, M.E. Wagshul, MR imaging and spectroscopy using hyperpolarized ^{129}Xe gas: preliminary human results, Magn. Reson. Med. 37 (1997) 809–815.

[8] J.R. MacFall, H.C. Charles, R.D. Black, H. Middleton, J.C. Schwartz, B. Saam, B. Driehuys, C. Erickson, W. Happer, G.D. Cates, G.A. Johnson, V.E. Ravin, Human lung air spaces: potential for MR imaging with hyperpolarized He-3, Radiology 200 (1996) 553–558.

[9] M. Salerno, T.A. Altes, J.P. Mugler III, M. Nakatsu, H. Hatabu, E.E. de Lange, Hyperpolarized noble gas MR imaging of the lung: potential clinical applications, Eur. J. Rad. 40 (2001) 33–44.
[10] M. Salerno, E.E. de Lange, T.A. Altes, J.D. Truwit, J.R. Brookeman, J.P. Mugler III, Emphysema: hyperpolarized helium 3 diffusion MR imaging of the lungs compared with spirometric indexes—initial experience, Radiology 222 (2002) 252–260.
[11] V. Callot, E. Canet, J. Brochot, Y. Berthezene, M. Viallon, H. Humblot, A. Briguet, H. Tournier, Y. Cremillieux, Vascular and perfusion imaging using encapsulated laser-polarized helium, MAGMA 12 (2001) 16–22.
[12] M.S. Chawla, X.J. Chen, G.P. Cofer, L.W. Hedlund, M.B. Kerby, T.B. Ottoboni, G.A. Johnson, Hyperpolarized ^{3}He microspheres as a novel vascular signal source for MRI, Magn. Reson. Med. 43 (2000) 440–445.
[13] M.S. Chawla, X.J. Chen, H.E. Möller, G.P. Cofer, C.T. Wheeler, L.W. Hedlund, G.A. Johnson, In vivo magnetic resonance vascular imaging using laser-polarized ^{3}He microbubbles, Proc. Natl. Acad. Sci. USA 95 (1998) 10832–10835.
[14] V. Callot, E. Canet, J. Brochot, M. Viallon, H. Humblot, A. Briguet, H. Tournier, Y. Cremillieux, MR perfusion imaging using encapsulated laser-polarized ^{3}He, Magn. Reson. Med. 46 (2001) 535–540.
[15] M.E. Wagshul, T.M. Button, H.F. Li, Z. Liang, C.S. Springer, K. Zhong, A. Wishnia, In vivo MR imaging and spectroscopy using hyperpolarized ^{129}Xe, Magn. Reson. Med. 36 (1996) 183–191.
[16] S.D. Swanson, M.S. Rosen, B.W. Agranoff, K.P. Coulter, R.C. Welsh, T.E. Chupp, Brain MRI with laser-polarized ^{129}Xe, Magn. Reson. Med. 38 (1997) 695–698.
[17] M.S. Albert, V.D. Schepkin, T.F. Budinger, Measurement of ^{129}Xe T1 in blood to explore the feasibility of hyperpolarized ^{129}Xe MRI, J. Comput. Assist. Tomogr. 19 (1995) 975–978.
[18] A. Bifone, Y.-Q. Song, R. Seydoux, R.E. Taylor, B.M. Goodson, T. Pietrass, T.F. Budinger, G. Navon, A. Pines, NMR of laser-polarized xenon in human blood, Proc. Natl. Acad. Sci. USA 93 (1996) 12932–12936.
[19] H.E. Möller, M.S. Chawla, X.J. Chen, B. Driehuys, L.W. Hedlund, C.T. Wheeler, G.A. Johnsson, Magnetic resonance angiography with hyperpolarized ^{129}Xe dissolved in a lipid emulsion, Magn. Reson. Med. 41 (1999) 1058–1064.
[20] G. Duhamel, P. Chouquet, E. Grillon, L. Lamalle, J.-L. Leviel, A. Ziegler, A. Constantinesco, Xenon-129 MR imaging and spectroscopy of rat brain using arterial delivery of hyperpolarized xenon in a lipid emulsion, Magn. Reson. Med. 46 (2001) 208–212.
[21] J. Wolber, I.J. Rowland, M.O. Leach, A. Bifone, Perfluorocarbon emulsions as intravenous delivery media for hyperpolarized xenon, Magn. Reson. Med. 41 (1999) 442–449.
[22] K. Golman, O. Axelsson, H. Johannesson, S. Månsson, C. Olofsson, J.S. Petersson, Parahydrogen-induced polarization in imaging: subsecond ^{13}C angiography, Magn. Reson. Med. 46 (2001) 1–5.
[23] L. Zhao, R. Mulkern, C.-T. Tseng, D. Williamson, S. Patz, R. Kraft, R.L. Walsworth, F.A. Jolesz, M.S. Albert, Gradient-echo imaging considerations for hyperpolarized ^{129}Xe MR, J. Magn. Reson. B 113 (1996) 179–183.
[24] J.-H. Gao, S.K. Holland, J.C. Gore, Nuclear magnetic resonance signal from flowing nuclei in rapid imaging using gradient echoes, Med. Phys. 15 (1988) 809–814.
[25] F. Ståhlberg, A. Ericsson, B. Nordell, C. Thomsen, O. Henriksen, B.R.R. Persson, MR imaging flow and motion, Acta Radiol. 33 (1992) 179–200.
[26] J.-H. Gao, L. Lemen, J. Xiong, B. Patyal, P.T. Fox, Magnetization and diffusion effects in NMR imaging of hyperpolarized substances, Magn. Reson. Med. 37 (1997) 153–158.
[27] M.A. Hemminga, Measurements of flow characteristics using NMR, in: T.L. James, A. Margulis (Eds.), Biomedical Magnetic Resonance, Radiology and Education Foundation, San Francisco, 1984, pp. 157–184.
[28] J.F. Himm, The solubility of xenon in simple organic solvents and in aqueous amino acid solutions, Thesis, Michigan State University, 1986.
[29] H. Gudbjartsson, S. Patz, The rician distribution of noisy MRI data, Magn. Reson. Med. 34 (1995) 910–914.
[30] M. Viallon, Y. Berthezene, M. Decorps, M. Wiart, V. Callot, M. Bourgeois, H. Humblot, A. Briguet, Y. Cremillieux, Laser-polarized (3)He as a probe for dynamic regional measurements of lung perfusion and ventilation using magnetic resonance imaging, Magn. Reson. Med. 44 (2000) 1–4.